4

Review of Adult Foot Radiology

LAWRENCE OSHER

In the workup of a hallux valgus deformity the practitioner is often faced with unexpected radiographic findings. Usually, the first course of action is to order additional pedal studies, which may provide the additional detail needed to help resolve or localize the apparent pathology. If the problem is within the purview of conventional radiography, a library text, if available, is often hurriedly consulted.

It is clearly not possible to encompass all of pedal radiology within the confines of a single chapter of this volume. Designed for the physician already familiar with basic musculoskeletal radiographic terminology, the following information will serve as a handy outline of foot pathology that may be encountered in the routine workup of the patient with hallux valgus deformity. Particular effort has been given to simplify the process of generating basic differential diagnoses. Pictorial examples are provided throughout this chapter.

RECOMMENDED APPROACH TO THE PEDAL RADIOGRAPH

Basic radiographic findings are not necessarily commonly seen. Their correct description, utilizing objective radiologic terminology and subsequent categorization, is vital to the generation of an appropriate differential. Traditional radiographic approaches often prescribe that, for every bone lesion, the following disease categories must be routinely considered:

Developmental anomalies
Trauma
Dysplasias and dysostoses
Metabolic disease (dystrophies included)
Infections and inflammatory processes
Tumor and tumor-like conditions
Degenerative disease and ischemic necrosis

However, this approach is presumptive; not only is an understanding of these basic bone radiographic changes clearly required, but one is expected to identify and then classify any lesion(s). Many radiographic bony abnormalities simply cannot be categorized at first glance by the average physician, despite the ability to correctly describe the basic pathologic changes. For these practitioners, a more intuitive approach utilizing clinical and laboratory data is required (studies clearly show improved accuracy in the reading of radiographs when appropriate clinical and laboratory data are provided). The following steps are recommended:

1. Identify the given views.
2. Discern *normal* from *abnormal* by describing any pathology in standard objective radiographic terminology.
3. Note available clinical and laboratory data.
4. Synthesize objective radiographic findings (item 2, above) with the significant clinical and laboratory data (3) to designate a spectrum of possible disease states in which both the radiographic and the clinical data could occur.
5. Rank individual diseases of this spectrum (4) as to their probability of occurrence, that is, most likely to least probable. This is the essence of differential diagnosis.
6. Suggest additional radiographic or other studies that might assist further in the differential diagnosis.

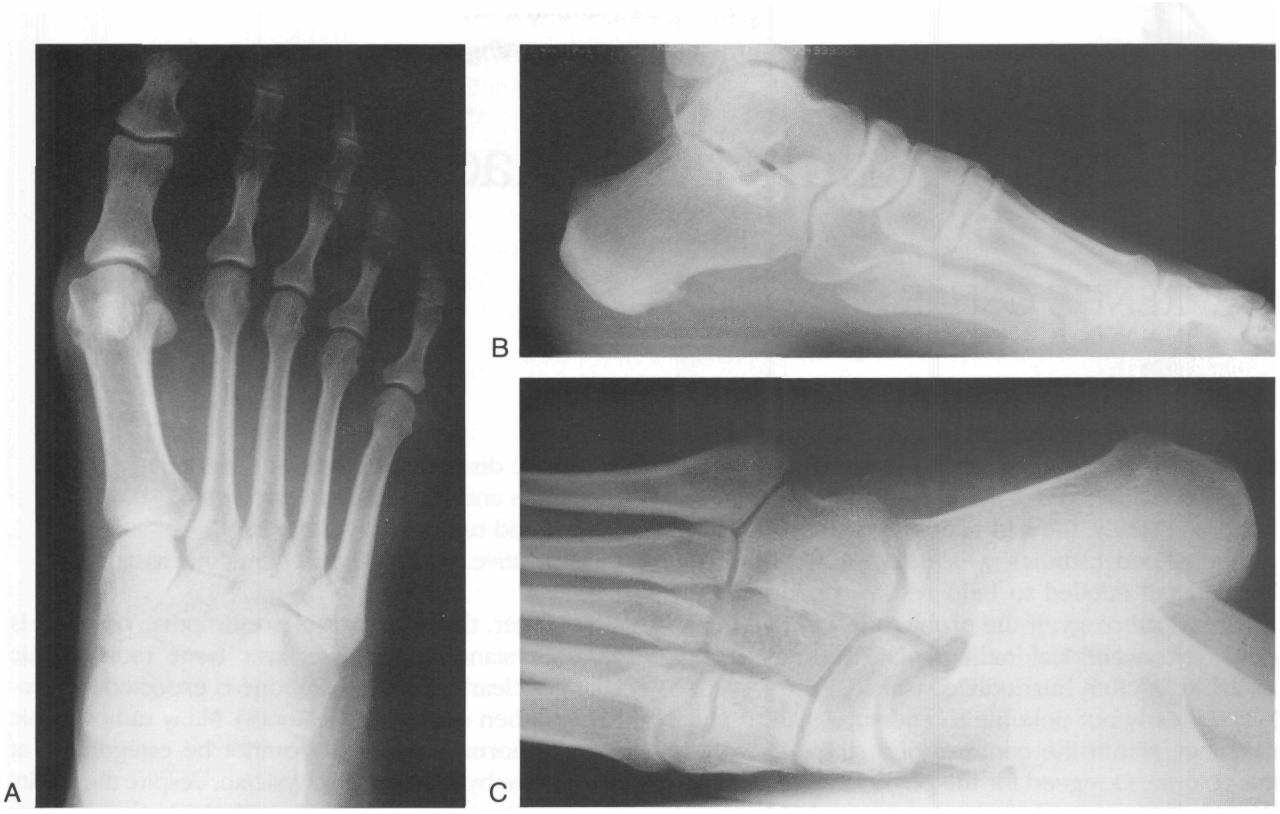

Fig. 4-1. (A) Reference anteroposterior view. **(B)** Reference lateral view. **(C)** Thirty-degree medial oblique foot view demonstrating incomplete calcaneonavicular coalition. Note separation between second and third cuneiforms.

A standard bone survey should be ordered whenever there is suspicion of multiple areas of involvement other than the foot. The standard bone survey comprises these radiographs:

Two views of skull
Two views of lumbar or thoracic spine
Anteroposterior view of pelvis
Anteroposterior views of arms and thighs

REVIEW OF INDICATIONS FOR THE BASIC ADJUNCT PEDAL VIEWS

It will be helped to first study the reference anteroposterior (Fig. 4-1A) and reference lateral views (Fig. 4-1B) before reviewing the following lists.

1. Medial oblique (-15° to 30°) (Fig. 4-1C)
   - Jone's fracture/base of fifth metatarsal
   - Lateral digits
   - Posterolateral talar process
   - Most accessory bones *except* os tibial externum
   - Lesser metatarsal head and base pathology
   - Lateral plantar calcaneus/foraminae
   - Subungual exostosis
   - Fibular sesamoid (10° study)
2. Isherwood medial oblique 45°-60°. This view will not visualize middle subtalar joint detail (Fig. 4-2).
   - Anterior facet of talocalcaneal joint
   - Anterior process os calcis
   - Calcaneonavicular coalition
   - Steidas process of talus
3. Lateral oblique (15°-30°) (Fig. 4-3)
   - Accessory navicular (os tibial externum)
   - Haglund's disease/navicular pathology
   - Cornuate/“gorilloid” navicular

Fig. 4-2. Isherwood medial oblique demonstrating normal shape of anterior calcaneal process. Note separation between third cuneiform and cuboid bones.

Fracture medial cuneiform
First metatarsophalangeal joint (MPJ) and medial hallux detail
Possible talonavicular coalition
Subungual exostosis/osteochondroma distal phalanx
Tibial sesamoid bone (45°-60°)

4. Hallux lateral
   Skyline hallux
   Distraction, sesamoid fracture at MPJ
   Interphalangeal sesamoid
   Subungual exostoses and osteochondroma
   Plantar cortex of distal phalanx
5. Harris-Beath (Fig. 4-4A)
   T-C coalitions (Fig. 4-4B), posterior and middle facet evaluation. (The anterior facet *cannot* be visualized adequately.)
   Coronoaxial skyline of the sustentaculum tali.
   Fractures of the os calcis, to evaluate posterior facet for longitudinal split as well as calcaneal foreshortening. These may be combined with various oblique axial views (Broden, Anthonsen, etc.).
   Arthritic changes of the subtalar joint.
6. Calcaneal axial
   Skyline of os calcis, which images cortical loss, protrusions, or promontories. The subtalar joint is not imaged.
   True space occupying lesions of the calcaneal body should be discriminated from a pseudocystic foramen calcaneum.
   Varus deformity of os calcis.
   Post trauma to rearfoot.
7. Forefoot (sesamoid) axial (Fig. 4-5A)
   Hypertrophic plantar metatarsal condyles
   Structural abnormalities of metatarsals, best visualized in coronal plane
   Changes to cristae
   Differentiation of symmetrically placed medial first metatarsal head erosions from cysts (Fig. 4-5B)
   Sesamoid detail
   Fractures
   Arthritic changes (cysts, erosions, bony proliferations, fusions)
   Sesamoid position (preoperative evaluation)
   Foreign bodies in plantar forefoot
   Base of metatarsal bones

THE BASIC PEDAL RADIOGRAPHIC DIFFERENTIALS

The following section is intended as a summation of commonly encountered pathologic conditions in pedal radiology. Topics such as bone tumors and con-

Fig. 4-3. Lateral oblique foot study.

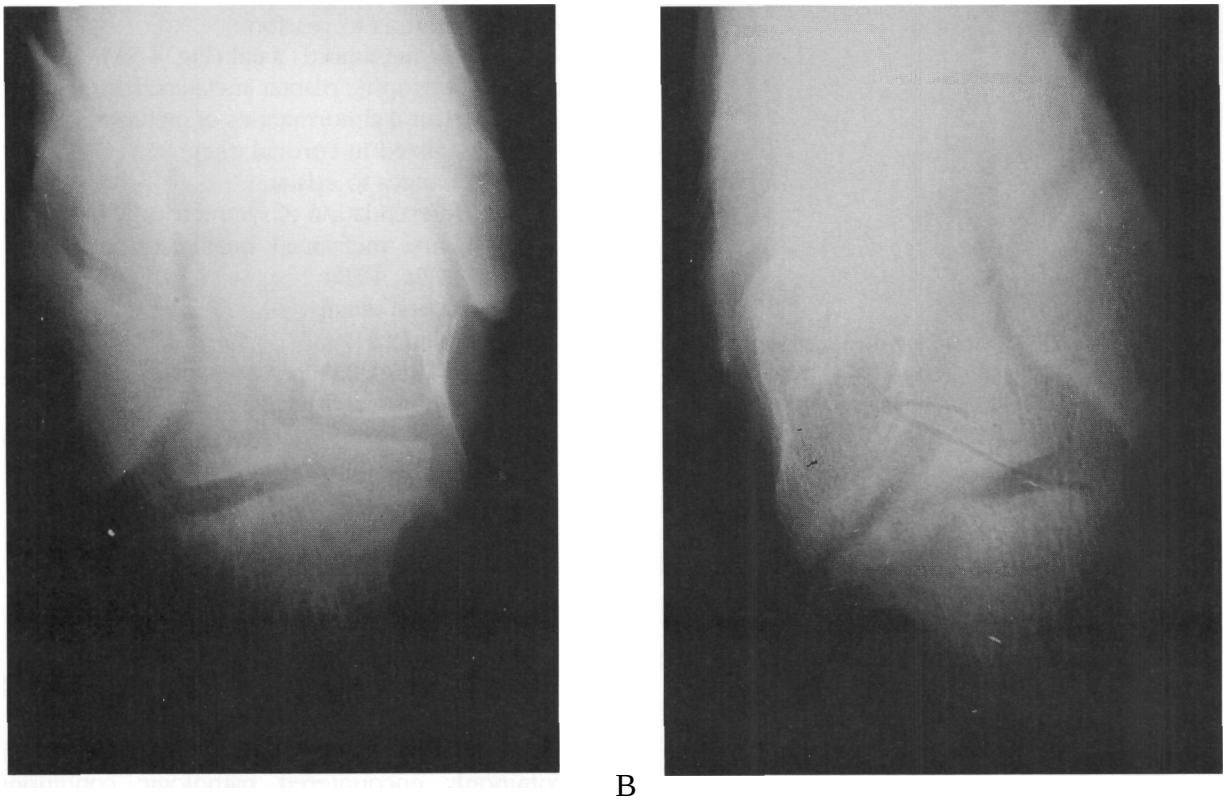

A B

Fig. 4-4 (A) Normal Harris-Beath study. **(B)** Harris-Beath view of a middle facet subtalar joint coalition.

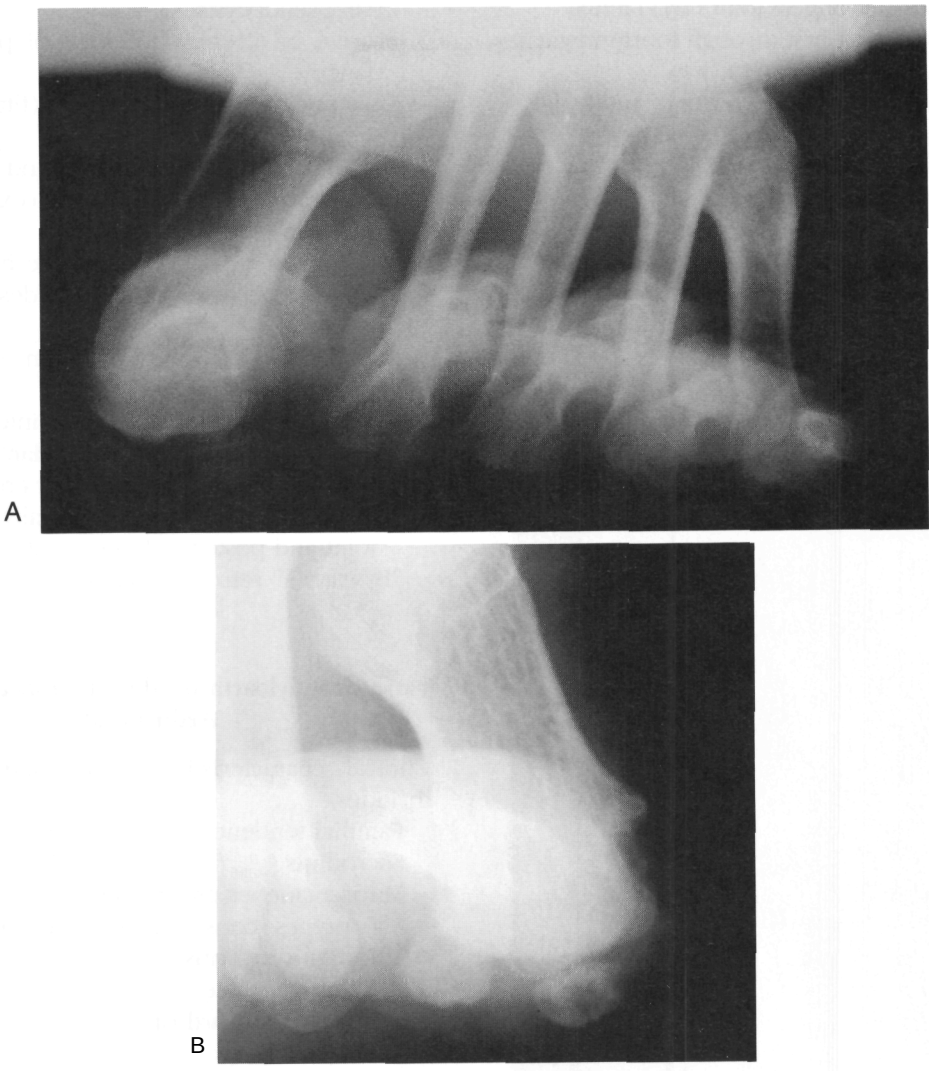

Fig. 4-5. (A) Normal forefoot axial study. **(B)** Magnification of forefoot axial study showing large (10.0-mm.) medial first metatarsal head erosion in a patient with chronic gouty arthritis. Note cystic/erosive change tibial sesamoid bone.

genital disorders are beyond the scope of this chapter and are not included.

The Common Arthropathies

Adult Rheumatoid Arthritis

1. General features

Articular complaints of the small joints of hands and feet; initial pedal onset occurs in approximately 15 percent of patients. These may be asymmetric initially, but eventually are bilaterally and symmetrically distributed in the joints.

Remissions and exacerbations may occur, with the remission period not exceeding 3 months.

Occurrence is bilateral and symmetrical.

Typical forefoot target zones

Fifth MPJ, most common medically and laterally

Medial interphalangeal joint (IPJ) hallux
Medial aspects of first through fourth metatarsal heads

2. Early radiographic features (predominantly MPJs (metatarsal heads) and medial IPJ hallux)
   Fusiform soft tissue swelling
   Juxta-articular osteopenia
   Concentric joint space narrowing
   Small para-articular cystic erosions (<5 mm)
3. Progressive forefoot radiographic findings (Fig. 4-6)

Fig. 4-6. Progressive forefoot radiographic changes. Extensive erosive changes are noted of the first, second, third, and fifth metatarsal heads. In addition, the medial aspect of the hallux IP joint is involved. Note the absence of PIP and DIP joint involvement and presence of cyst formation on fifth metatarsal head.

Cysts/pseudocysts
Erosive involvement of base of proximal phalanges
Osseous "island" formation (fifth metatarsal head)
Digital deformities; deviations and subluxations
Nonosseous (fibrous) ankylosis (exceptions; carpus and tarsus)

4. Midfoot and rearfoot radiographic findings (forefoot involvement typically precedes rearfoot by many years)
   Rigid flatfoot deformity common
   Bony ankylosis of tarsal joints
   Concentric narrowing of tarsal/intertarsal joints, which may lack juxta-articular osteoporosis and typically lack periarticular erosive changes
   Secondary osteoarthritis, especially talonavicular joint and posterior facet of subtalar joint
   "Bywater's" retrocalcaneal bursal lytic lesions

Spondyloarthropathies (Seronegative Arthritides)

1. Clinical characteristics of the seronegative arthritides
   Familial tendency
   Sacroiliitis
   Mucocutaneous affectations
   Major types (considerable clinical overlap exists)
      Psoriatic arthritis
      Reiter's disease
      Enteropathic arthritis
      Ankylosing spondylitis
   Target sites
      Early digital and heel involvement with enthesopathic findings
      MPJs, proximal interphalangeal joints (PIPJs), and distal interphalangeal joints (DIPJs)
      Hallucal sesamoids
      Calcaneus, ankle and knee joints
2. Pedal radiographic changes of seronegative arthritis (Figs. 4-7 to 4-10)
   Early changes soft tissues are nonspecific.
   Asymmetric dactylitis (Fig. 4-7) exhibits profound fusiform digital soft tissue swelling secondary to joint effusions, and flexor tenosynovitis with or without periostitis.

Fig. 4-7. Asymmetric dactylitis with periostitis of second and fourth toes in a patient with Reiter's disease.

Underlying osseous changes may be present in approximately 50 percent of patients.
Periosteal apposition adjacent to symptomatic joints and tendoligamentous attachments occurs during symptomatic periods.
Osteosclerosis is common but osteoporosis is lacking.
Poorly defined juxta-articular erosions are common with marginal "whiskering periostitis."
Intra-articular bony ankylosis is also common, especially psoriatic arthritis (Fig. 4-8).
Joint space narrowing is uniform.
Acrolysis is present (Fig. 4-9).
Minimal cyst formation occurs.
Erosive and proliferative bony calcaneal changes occur (Fig. 4-10).

3. General comparison of adult rheumatoid arthritis versus seronegative arthritis
   Seronegative arthritis lacks nodules.
   Bilateral asymmetric presentation is common in seronegative arthritis (oligoarticular).
   These following joints are uncommonly involved in adult rheumatoid arthritis:
      DIPJs
      PIPJs (in foot only)
      Sacroiliac (SI) joints (symmetric)
      Thoracolumbar joint
   Dactylitis and enthesopathies are common (initial) complaints in seronegative arthritis; early heel complaints occur in seronegative arthropathies.
   Seronegative arthritis often lacks profound osteopenia.
   Seronegative arthritis lacks significant cystic degeneration.
   Rheumatoid arthritis lacks periostitis and acrolysis.
   Medial, lateral, and central erosive changes to IP hallux occur in rheumatoid arthritis.

Psoriatic Arthritis

1. Correlative clinical data of psoriatic arthritis
   Good correlation between nail changes and arthritis (not skin)
   Bilateral asymmetric oligoarthritis
   Five patterns of arthritic attack
      Asymmetric oligoarthritis (70 percent)
      Symmetric polyarthritis (15 percent)
      DIP joint only (5 percent)
      Arthritis mutilans (5 percent)
      Ankylosing spondylitis (5 percent)
   Target sites
      IP hallux (considered the most destructive arthropathy of the hallucal IP joint)
      PIPs, DIPs, and MPs
      Sesamoids
      Calcaneus (Resnick's sites 2-5)
      Ankle joint
2. Radiographic changes of psoriatic arthritis in foot
   Normodensity or osteopenia seen during acute phases (typically ephemeral)

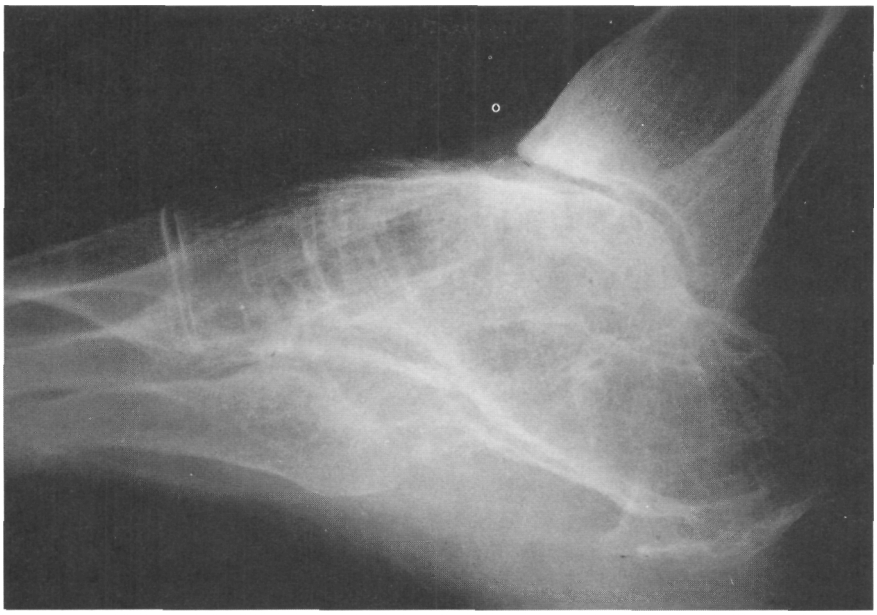

Fig. 4-8. Generalized bony ankylosis along with a large "fluffy" infracalcaneal spur in a patient with mutilating psoriatic arthritis.

Bony ankylosis of DIPJs, PIPJs, and MPJs as well as tarsal bones (Note: As many as 30 percent of joints in psoriatic arthritis fuse) (Fig. 4-8)
Joint space widening and narrowing
Subchondral sclerosis
Localized osteosclerosis
Marginal joint "mouse-ear" erosions that may be obscured by periosteal reaction
Resorption and proliferative osseous changes that may lead to arthritis mutilans with typical "pencil-and-cup" deformities or to digital contractions/subluxations
"Ivory phalanx syndrome," or profound osteosclerosis of hallucal distal phalanx secondary to condensation of bone on periosteal and endosteal surfaces (Fig. 4-9)
Generalized sclerosis of os calcis and large, poorly defined "fluffy" spurs during symptomatic periods
Asymmetric digital dactylitis (Fig. 4-7)
Distal phalangeal tuft resorption (acro-osteolysis) (Fig. 4-9)

Reiter's Disease

1. Correlative clinical data of Reiter's disease
   - Young males
   - Urethritis (typically nongonococcal) or enteritis
   - Conjunctivitis
   - Mucocutaneous lesions
     - Keratodermia blennorrhagicum
     - Balanitis
     - Mouth
   - Arthritis
     - Not common in upper extremities
     - Dactylitis or heel pain a common initial complaint
     - Joint deformity not as severe as in psoriatic arthritis
     - Forefoot joint involvement typically monoarticular
     - End-stage arthritis mutilans rare (Launois' deformity)
   - Pedal target sites
     - MTP joints

Fig. 4-9. Psoriatic arthritis. Visible is an "ivory" osteosclerotic distal phalanx of hallux. Note the acrolysis as well as intra-articular bony ankylosis of the IP joint.

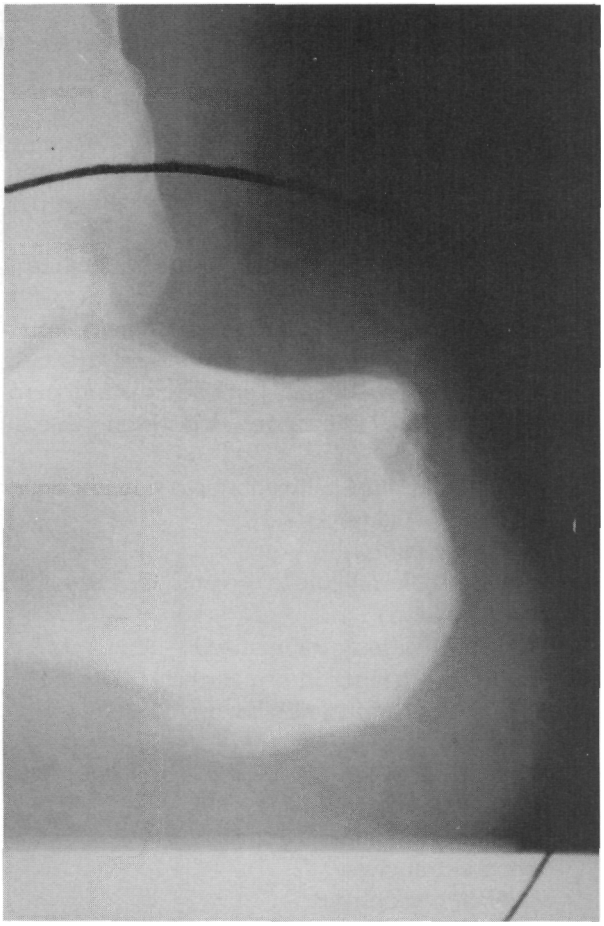

Fig. 4-10. Seronegative heel showing typical erosive finding of retrocalcaneal bursal area and also large "fluffy" heel spur at infracalcaneal attachment of plantar fascia/intrinsics. Note generalized sclerosis of os calcis.

First IP joint, medial and lateral
Calcaneus
Achilles tendon
Ankle joint

2. Radiographic features of Reiter's disease versus psoriatic arthritis
   - Except for the hallux IP joint, DIP and PIP joint involvement is not as common as in psoriatic arthritis.
   - There is a greater tendency for osteopenic changes in Reiter's, particularly during acute phases (which last longer). Normal mineralization then returns.
   - There is also a lesser tendency for bony ankylosis in Reiter's disease.
   - Early loss of retrocalcaneal recess along with achilles tendon swelling is common; subjacent erosive and proliferative calcaneal lesions (sites 1, 2, & 4) occur in Reiter's disease (Fig. 4-10).
   - Joint space widening is not uncommon in psoriatic arthritis.

Osteoarthritis (Degenerative Joint Disease)

1. Correlative clinical data of pedal Osteoarthritis
   - This is typically a secondary Osteoarthritis. It is commonly accepted that an association exists with pathomechanics/altered stress patterns

across joint(s) associated with the following:
First MPJ axis of motion/instant center alteration
Angle of metatarsus adductus
First ray pathomechanics with pronation
Sagittal plane elevation of first metatarsal/ray
Other typical forms of secondary pedal osteoarthritis
Trauma: osteochondritis dissecans, Freiberg's infraction, post sprains and fractures
Congenital: tarsal coalitions, hereditary multiple exostosis, multiple epiphyseal dysplasia
Arthritides: rheumatoid arthritis, calcium pyrophosphate dihydrate deposition disease (CPPD).
Iatrogenic: after hallux abducto valgus surgery
Common pedal target sites
First MP joint(s)
Medial column joints (greater mobility with pronation)
Joints previously traumatized

2. Radiographic changes in osteoarthritis (Fig. 4-11)
Unilaterally or bilaterally asymmetric
Minimal soft tissue signs
Asymmetric/focal (symmetric narrowing late) joint space narrowing
Subchondral sclerosis/eburnation
Subchondral cysts
Marginal osteophytes
Paucity of periarticular fragmentation
Absent erosions

Fig. 4-11. Typical osteoarthritic changes of the first metatarsophalangeal joint include focal narrowing, subchondral sclerosis, and marginal osteophytosis/proliferative changes including sesamoids.

Erosive Osteoarthritis

1. Key clinical data of erosive osteoarthritis
Occur predominantly in postmenopausal women
Pedal target sites most often IP joints
2. Radiographic changes in erosive osteoarthritis
Soft tissue swelling
Marginal osteophyte formation
Central joint space erosive changes producing a typical "seagull" appearance
Bony ankylosis common and may dominate radiographic picture

Gouty Arthritis

1. Correlative clinical data of gouty arthritis
Pedal target sites may involve any site in the foot.
First MPJ arthritis (65 percent initially, 90 percent at some time)
Hallux IP joint
Tarsometatarsal joint (see Fig. 4-13)
Ankle joint
2. Early radiographic changes (Fig. 4-12A)
Extreme periarticular soft tissue swelling
Significant osseous changes absent
Typically monoarticular
3. Late (chronic) changes
Joint space preserved until late
Asymmetric polyarticular (chronic)
Erosions (Fig. 4-12B and C)
Juxta-articular/para-anicular
May be extra-articular

Fig. 4-12. **(A)** Acute gouty arthritis of the first metatarsophalangeal joint. **(B)** Chronic gouty arthritis. Visible is a large erosive change of hallucal proximal phalanx (10.0 mm) that is clearly both extra-articular as well as periarticular. Note eccentric soft tissue tophae of IPJ and MPJ. **(C)** Large erosive change of medial hallucal proximal phalanx along with lateral erosive change at IP joint margin. These changes are unusual in adult rheumatoid arthritis. Note the subchondral density is normal.

Large size (often >5.0 mm) with "punched-out" appearance
Overhanging, proliferative margins (Martel's sign)
Sclerotic lining
Tophi (Fig. 4-12B)
Eccentric focal soft tissue masses typically with subjacent erosions (versus rheumatoid arthritis nodules)
May rarely become calcified
Subchondral bony density typically unchanged (normodensity)
Bony ankylosis and periostitis not overall prominent features
Osseous infarcts
End-stage osteolysis may mimic malignancy or somewhat resemble Charcot joint disease (especially when midfoot is involved) (Fig. 4-13)

Fig. 4-13. Extensive osteolysis base of fourth metatarsal bone in a patient with chronic gouty arthritis. The changes may otherwise resemble charcot joint arthropathy.

Systemic Lupus Erythermatosus

1. Correlative clinical data of systemic lupus erythermatosus (SLE)
Young females, increased incidence in blacks.
Deforming, nonerosive arthritis of two or more joints
Multisystem, including central nervous system (CNS) (seizures, etc.), pulmonary (effusions, pleuritis, etc.), renal (to 50 percent glomerulonephritis), cardiac, and skin (malar butterfly or discoid plaquelike scaling
Pedal target sites
MPJs
Terminal phalangeal tufts (occasionally)
2. Radiographic changes in SLE
Bilateral and symmetrical joint involvement
Soft tissue swelling
Juxta-articular osteopenia
Minimal/absent joint space narrowing
Deforming, nonerosive arthropathy involving MPJs (reversible) with subluxations and dislocations
Symmetric polyarthritis
Osteonecrosis/Freiberg-like deformities
Soft tissue calcifications
Occasional acrolysis of distal phalanges

Septic Arthritis

1. Correlative clinical data of septic arthritis
This is an acute, red, hot monoarticular arthritis.
It may occur secondary to hematogenous osteomyelitis in adults and infants or otherwise in certain joints in children where the metaphysis is intra-articular (e.g., hip).
Associated signs and conditions in adult patients
Debilitation
I.V. drug user
Prosthetic joint
Direct trauma
Contiguous osteomyelitis
Post gonorrheal infection

2. Radiographic changes in suppurative (pyogenic) arthritis
   - Soft tissue swelling about joint
   - Poorly marginated osseous erosions (peripheral periarticular "bare" areas and/or central involvement)
   - Central joint space erosions
   - Rapid (1-3 weeks) concentric chondrolysis/joint space narrowing
   - Reactive sclerosis (lacks osteopenia)
   - Eventual intra-articular bony ankylosis
   - Involvement of adjacent bony structures producing classic picture of osteomyelitis
3. Radiographic changes in nonsuppurative, tuberculous arthritis
   - Phemister's triad
     - Gradual (slow) loss of joint space
     - Juxta-articular osteoporosis
     - Peripheral osseous erosions
   - Subchondral osseous erosions, central and peripheral (peripheral are seen more often in hip/knee/ankle)
   - Tendency toward fibrous ankylosis
   - Late joint space loss
   - Less periostitis than pyogenic and gonorrheal
4. Correlative clinical data of gonococcal arthritis
   - Male > female
   - Onset sudden or insidious
   - Days 1 to 3
     - Systemic signs/symptoms
     - Rash and fever/chills
   - Days 4 to 6
     - Pauciarticular or polyarticular
     - Small joints of foot
     - Enthesopathy, calcaneous
     - Knee > ankle > wrist > shoulder > foot > spine
     - Lower extremities > upper extremities
   - Associated with multiple joints and tenosynovitis
5. Radiographic findings in gonococcal arthritis
   - As with pyogenic if untreated
   - Osteoporosis and soft tissue swelling if treated

Charcot Joint Arthropathy

1. Differential diagnosis of disorders that may produce a radiographic picture of neuropathic joint disease
   - Diabetes mellitus
   - Tertiary syphilis
   - Congenital indifference to pain
   - Other neuropathic etiologies
     - Syringomyelia
     - Spina bifida
     - Charcot-Marie-Tooth disease (rare)
     - Post-trauma
   - Pyrophosphate arthropathy (talonavicular joint)
   - Idiopathic osteonecrosis of navicular
   - Avascular necrosis of talus
   - Hemophilia
   - Primary amyloidosis
   - Post sympathectomy
2. Correlative clinical data of diabetic Charcot joint arthropathy
   - About 1 percent incidence among diabetic patients
   - Signs typically worse than symptoms
   - Soft tissue swelling with increased range of motion (ROM) and subsequent decreased ROM often with crepitus
   - Associated with long-standing diabetes, poor control, and diabetic neuropathy
   - Pedal target sites
   - Weight-bearing "hypertrophic":
     - Ankle joint (Fig. 4-14)
     - Lisfranc's joint (Fig. 4-15.)

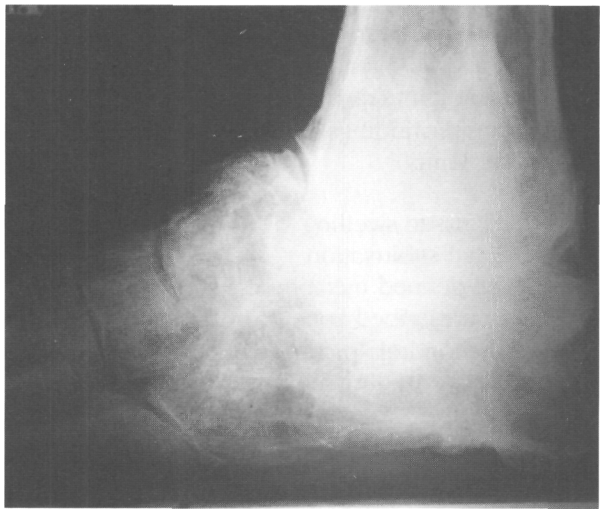

Fig. 4-14. "Hypertrophic" Charcot joint deformity of the ankle in a patient with underlying neuropathy.

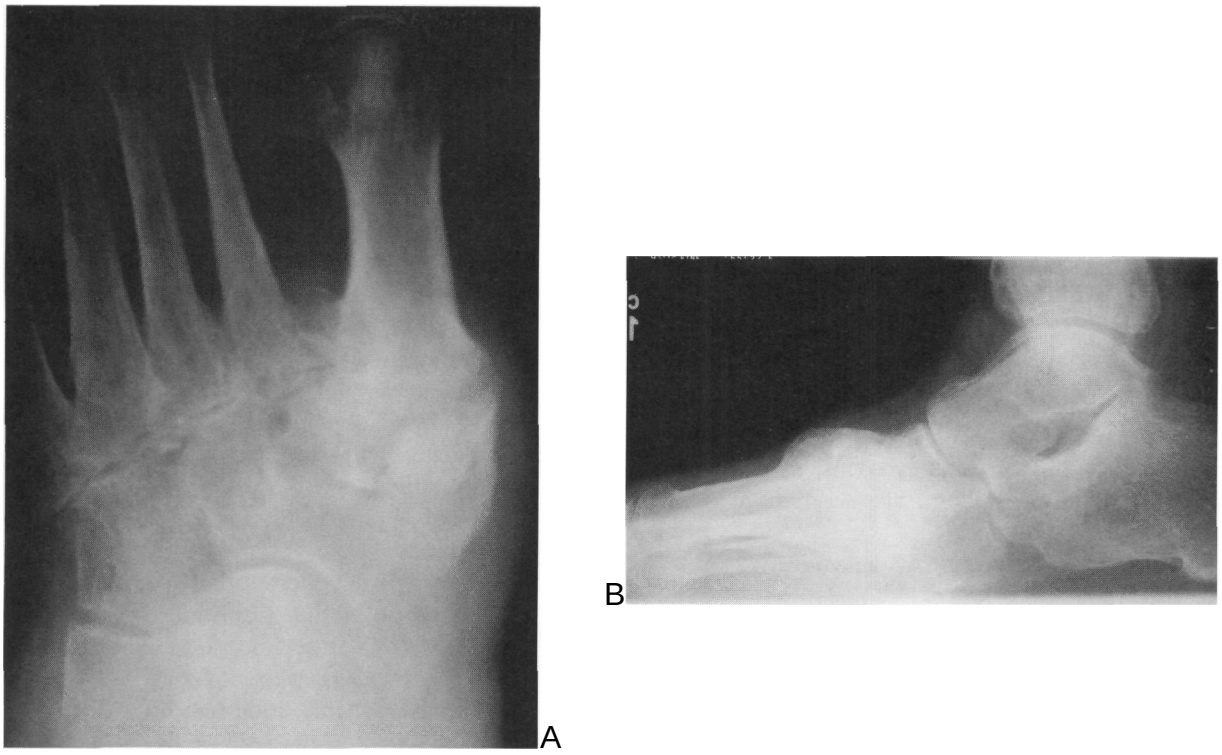

Fig. 4-15. (A) Anteroposterior view of hypertrophic Charcot joint deformity of Lisfranc's joint with resultant cube-foot deformity. (B) Lateral view of cube-foot deformity (same patient as in Fig. 4-15A).

Chopart's joint
Subtalar joints (rarer)
Non-weight-bearing atrophic:
IP and MP joints
Ankle joint (rare)

3. Radiographic findings in diabetic neuroarthropathy (Charcot joints)
Early
Soft tissue swelling
Digital subluxation
Well-defined metaphyseal cortical defects
Circumscribed zone of osteopenia
Subchondral "picture-framing" osteopenia
Possible underlying fracture
Progressive
Poorly defined metaphyseal cortical defects
Periosteal reaction
Extensive osseous erosion and lysis (Fig. 4-16A)
Fragmentation

Note: The radiographic changes in this stage mimic acute, direct-extension osteomyelitis. However, the presence of osteopenia and lysis suggests an intact vascular supply, and should not be misconstrued as a criterion to amputate.

Late, with significant weight-bearing (see Figs. 4-14 and 4-15)
Generalized sclerosis adjacent to site
Variable joint space narrowing
Extensive osseous fragmentation
Hypertrophic "bulky" osteophytes
Severe destruction/disorganization
"Cube foot" forefoot abduction (Fig. 4-15A and B)
Occasional bony ankylosis

Late, without significant weight-bearing (Fig. 4-16B)
Sclerotic "pointed tubular bone" deformity with diaphyseal sparing

Fig. 4-16. (A) Progressive stage of diabetic osteolysis of the fifth toe. These changes are radiographically indistinguishable from acute osteomyelitis (direct-extension type). **(B)** End-stage pointed tubular bone deformities in a patient with underlying neuropathy.

Overt osteolysis
Restitution of integrity (forefoot)
Arthritis mutilans
Ankylosis not uncommon

Diffuse Idiopathic Skeletal Hyperostosis

1. Correlative clinical data for diffuse idiopathic skeletal hyperostosis (DISH)
   Older than 50 years
   Common axial syndesmophyte disease with appendicular manifestations
   Males > females
   Benign nature of complaints; back stiffness with mild pain, talalgia, "tennis elbow," dysphagia
   Not a true arthropathy
   Pedal target areas, attachments of major soft tissue tendons and ligaments into bone (pure enthesopathy)
2. Pedal radiographic findings (Fig. 4-17), enthesopathic osseous spurring
   Common in dorsal midfoot
   Calcaneus: large, poorly defined osseous appositions frequent at all major attachment sites
   Base of fifth metatarsal
   Anteriomedial navicular

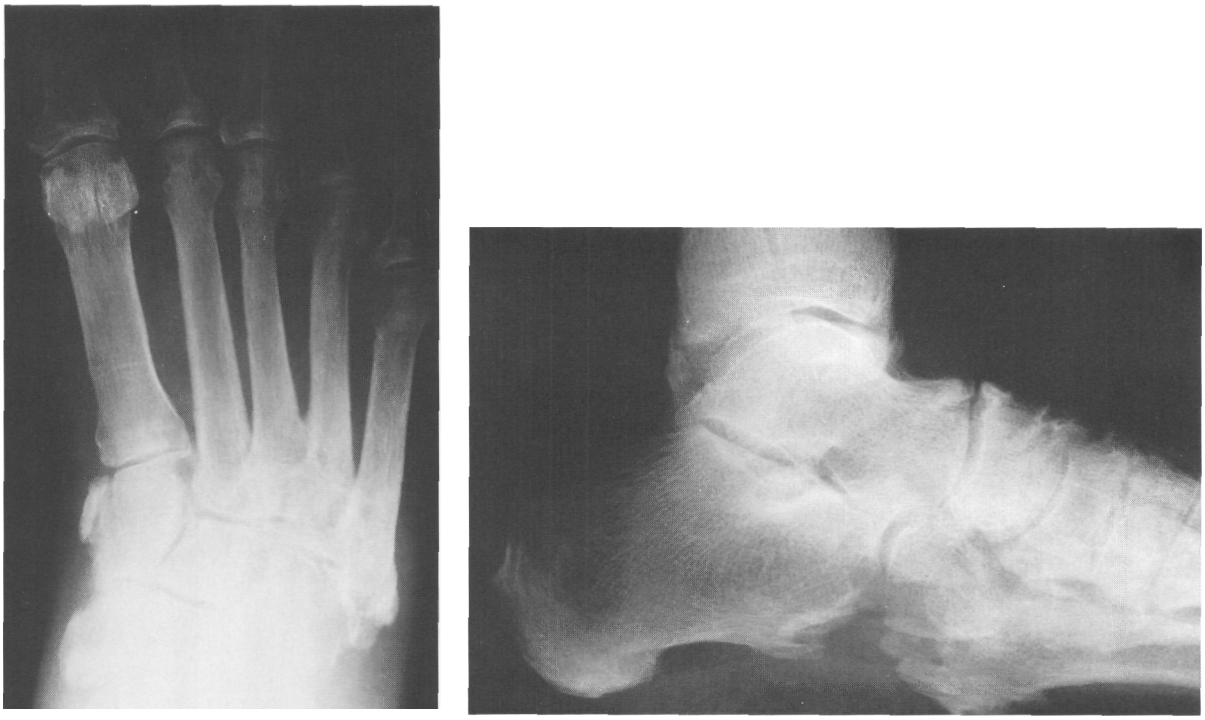

A B

Fig. 4-17. (A) Anteroposterior view of midfoot of 91-year-old woman with underlying diffuse idiopathic skeletal hyperostosis. Extensive osseous apposition is noted at attachments sites of the flexor hallucis brevis (sesamoids), peroneus brevis, and anterior tibial tendons. **(B)** DISH. This lateral view of same patient in Fig. 4-15A shows extensive dorsal midfoot spurring as well as calcaneal and deltoid ligamentous involvements.

Medial first cuneiform
Hallucal sesamoids
Forefoot joint capsular ossific spurring late (>75 years)
Metatarsal shafts (inconsistent)
Soft tissue ossification/calcifications not uncommon

3. Postoperative new bone formation of implants

Basic Differentials of "Solid" Periostitis

Solid periostitis is basically a reaction to some subperiosteal or extraperiosteal irritant. Common causes include the following:

Osteomyelitis
Arthritis (seronegative, etc)
Bone tumor
Reaction to chronic soft tissue inflammation
Reaction to trauma/hematoma subperiosteal space
Healing fracture.

Basic Differentials of Generalized (Symmetric) Solid Periostitis of Adults

1. Primary (familial, idiopathic) hypertrophic osteoarthropathy
   Radiographic
   Tarsals, metatarsals, and phalanges
   Diaphyseal/metaphyseal/epiphyseal
   "Shaggy" irregular periostitis (spiculated)
   Ligamentous ossification
2. Secondary hypertrophic osteoarthropathy (HOA) (Fig. 4-18)
   Underlying primary lesion (often bronchogenic cancer)

Fig. 4-18. (A & B) Secondary HOA. "Solid," linear periosteal new bone formation of metatarsal shafts 2, 3, and 4 bilaterally are seen in a patient with underlying oat cell lung carcinoma.

Joint symptoms and signs worse in 30 to 40 percent
Radiographic
Metatarsals and phalanges
Diaphyseal/metaphyseal
Often linear or laminated, regular or irregular periostitis
Periarticular osteoporosis and swelling
Differential diagnosis, DISH and juvenile rheumatoid arthritis

3. Thyroid acropachy
   Hyperthyroidism
   Clubbing
   Periostitis
   Exopthalmos
   Soft tissue swelling/myxedema
   Radiographic
   Diaphyseal
   Shaggy, spiculated periostitis
4. Hypervitaminosis A (may be residual in adults)
   Radiographic
   Metatarsals
   Diaphyseal only, periostitis
   Wavy or undulating cortical hyperostosis
   Other findings
   Epiphyseal, invagination and hypertrophy
   Metaphyseal widening, cupping, and shortening
   Premature closure of growth plates
5. Vascular insufficiency
6. Chronic venous stasis (tibial periostitis)
7. Polyarteritis nodosum
8. Tuberous sclerosis
9. Fluorosis
10. DISH (occasional)

Selected Disorders of Increased Tubular Bony Diameters (and also Acropachy)

1. Diaphyseal
   Acromegaly
   Paget's disease
2. Metaphyseal
   Osteopetrosis (osteosclerotic)
   Pyle's disease (no osteosclerosis)
   Gaucher's disease (no osteosclerosis)

Shortened Tubular Bone Deformities (Brachydactyly)

1. Hallux
   - Diabetic neurotrophic osteoarthropathy
2. Phalanges and metatarsals
   - Diabetic neurotrophic osteoarthropathy
   - Idiopathic, isolated anomaly
   - Rheumatoid arthritis
   - Pseudohypoparathyroidism (especially first and fourth metatarsals)
   - Pseudopseudohypoparathyroidism
   - Turner syndrome (especially fourth metatarsal)
   - Basal cell nevus syndrome
   - Hereditary multiple exostoses
   - Juvenile rheumatoid arthritis
   - Infarction
   - Trauma (fracture, burn, etc.)
   - Sickle cell disease
3. Flattened metatarsal heads
   - Freiberg's infraction
   - Diabetic neurotrophic osteoarthropathy

Some Disorders of Decreased Tubular Bony Diameters

1. Acromegaly
2. Diabetic neuro-osteoarthropathy (DNOAP)
3. Juvenile rheumatoid arthritis
4. Congenital syphilis

Selected Pointed Tubular Bone Deformities

1. DNOAP
2. Psoriatic arthritis
3. Alcoholic neuroarthropathy
4. Scleroderma, dermatomyositis
5. Seronegative arthropathies
6. Buerger's disease (TAO)
7. Arteriosclerosis obliterans
8. Raynaud's disease

Acrolysis

1. Idiopathic
2. Scleroderma
3. Psoriasis (see Fig. 4-9)
4. Neuroarthropathy
   - Diabetes
   - Tabes dorsales
   - Syringomyelia
5. Hyperparathyroidism
6. Vascular
   - TAO
   - Raynaud's disease
7. Leprosy
8. Post Injury
   - Frostbite
   - Burns
9. Polyvinylchloride (PVC) workers
10. Dilantin and ergot therapy
11. Chronic gout (asymmetric)
12. Epidermolysis bullosa

"Bone Within a Bone" Appearance

1. Osteopetrosis
2. Sickle cell disease
3. Sickle cell-ß-thalassemia disease
4. Some heavy metal intoxications (e.g., phosphorus)
5. Chronic osteomyelitis
6. Congenital syphilis

Selected Sclerotic Disorders (Internal Osseous Disorders)

1. Transverse metaphyseal banding
   - Heavy metal (lead) poisoning
   - Osteopetrosis
   - Phosphorus osteopathy
   - Scurvy
   - Congenital syphilis (metaphysitis)
   - Hypervitaminosis A and D
   - Leukemia (acute)
   - Reinforcement lines of osteoporosis
2. Solitary circumscribed foci of osteosclerosis
   - Enostoses (bone islands)
   - Osteoid osteoma (medullary)
   - Osteoma
   - Focal infarct (Fig. 4-19)
   - Old nutrient foraminae (especially calcaneus)
   - Healed fibrous bone lesion
3. Multiple circumscribed foci of osteosclerosis
   - Osteopoikilosis
   - Gardner syndrome (osteomata)
   - Medullary fat necrosis/infarction

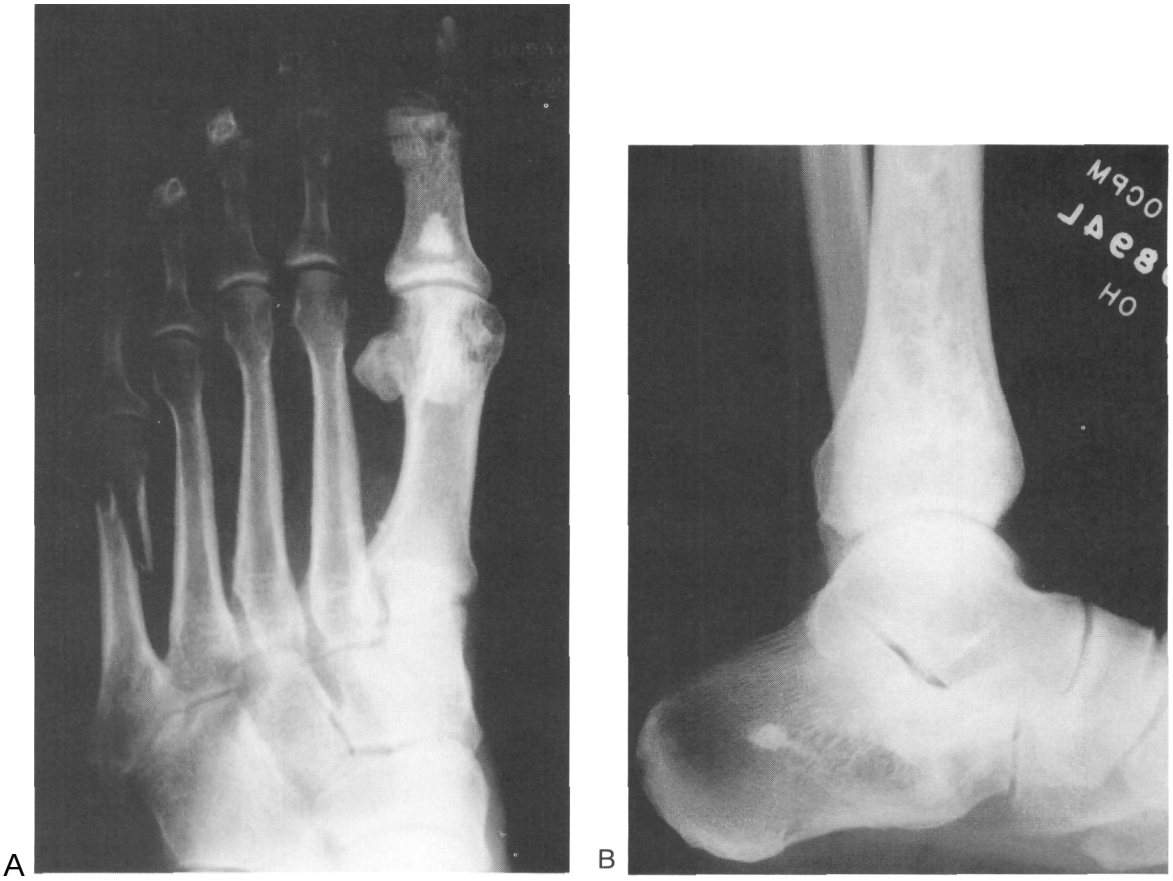

Fig. 4-19. (A) Base of hallucal proximal focal osteosclerotic infarct in a patient with alcoholic pancreatitis. **(B)** Focal osteosclerotic lesion of os calcis (same patient as in Fig. 4-19A). Considering the nonhealing fifth metatarsal fracture, sickle cell disease remained a primary disorder to rule out.

4. Patchy-diffuse osteosclerosis/sclerotic foci
   - Previous infarct (may have serpiginous qualities)
   - Endosteal fracture "callus"
   - Fibrous dysplasia
   - Sclerosing osteitis in infection
   - Chronic osteomyelitis
   - Osteoblastic metastases (breast, prostate)
   - Idiopathic osteonecrosis (navicular)
   - Paget's disease
   - Secondary hyperparathyroidism
   - Primary osteogenic bone tumors
   - Fairbank disease
   - Epiphyseal bone infarction:
     - Osteochondroses
     - Post-traumatic
     - Systemic lupus erythematosus
   - Metaphyseal bone infarction:
     - Sickle cell disease
     - Infiltrated collagen vasculitides diagnosis
     - Infections in juxtametaphyses
     - Pancreatitis (Fig. 4-20).
     - Steroids (pheochromocytoma)
     - Rheumatoid arthritis
   - Granuloma
5. Diffuse sclerosis of bones
   - Osteopetrosis/pycnodysostosis
   - Paget's disease
   - Hematopoietic disorders: mastocystosis, anemias, myelofibrosis, leukemias
   - Metastases
   - Hypervitaminosis A and D

Fig. 4-20. (A) Patchy-diffuse intramedullary osteosclerosis of the distal tibia. Osteosclerotic metatases must be ruled out. **(B)** Distal tibia (same patient as in Fig. 4-20A).

Hypo/pseudohypo- and pseudopseudohypoparathyroidism
Fluorosis
Melorheostosis
Chronic osteomyelitis

Selected Osteopenic Disorders

1. Subperiosteal resorption (rapid)
   Hyperparathyroidism
   Reflex sympathetic dystrophy syndrome (RSDS)
   Tendon avulsion (e.g., cortical desmoid)
2. Spotted deossification (rapid)
   Reflex sympathetic dystrophy syndrome (RSDS) (Fig. 4-21)
   Disuse osteoporosis (occasionally)
3. Generalized/nonregional (*, pediatric)
   Senile osteoporosis
   Osteomalacia (osteoporosis with bending)
   Rickets (osteoporosis with bending)*
   Chronic alcoholism
   Malabsorption/malnutrition
   Vitamin C (scurvy) deficiency*
   Neuromuscular diseases/cerebral palsy
   Osteogenesis imperfecta*
   Endocrine:
      Hyperparathyroidism/Renal Osteodystrophy*
      Hypogonadism
      Diabetes mellitus (long-standing, poor control)
      Cushing's disease
      Hyperthyroidism

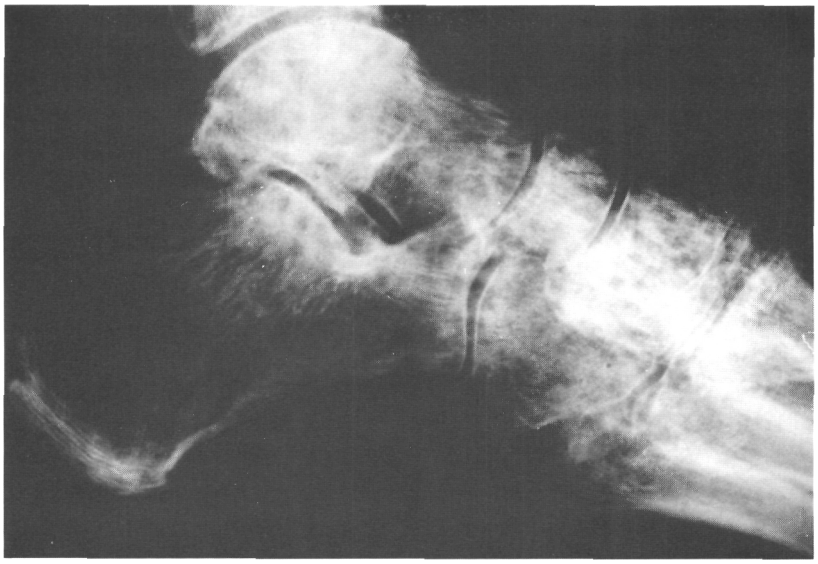

Fig. 4-21. "Spotty" juxta-articular or cancellous bony deossification in a patient with underlying reflex sympathetic dystrophy syndrome.

Hypothyroidism
Collagen diseases
Chronic anemias (e.g., iron deficiency)*
Multiple myeloma
Metastatic disease
Iatrogenic (steroids, heparin therapy)

4. Localized osteopenia
   RSDS (may be seen as early as 3-4 weeks)
   Post-traumatic disuse/immobilization atrophy (seen at about 8-10 weeks)
   Note: Hawkin's sign, a favorable radiographic sign suggesting the potential to heal, is merely the presence of a thin zone of *subchondral* lucency of the talar dome at a time (usually 8—10 weeks post trauma) when disuse osteoporosis is radiographically apparent elsewhere.
   Paget's disease (lytic phase I)
   Regional migratory osteopenia
   Tumor
   Juvenile rheumatoid arthritis
   Early osteomyelitis (Fig. 4-22)
5. Multiple radiolucencies, primarily in multiple metaphyses (modulation of normal growth pattern at the epiphyseal plate and metaphyseal junction)
   Congenital syphilis
   Hypervitaminosis A, excess osteoclastic activity in metaphysis with active new bone proliferation in diaphysis
   Hypovitaminosis C, scurvy (Barlow's disease)
6. Reticular areas of radiolucency
   Sickle cell anemia
   Anemias, thalessemia
7. Regional osteopenic disorders/speckled or patchy multiple radiolucencies (may mimic "moth-eaten" destruction; typically involve cancellous bone)
   Reflex sympathetic dystrophy syndrome (RSDS)
   Rapidly forming osteoporoses
8. Focal osteopenia
   Internal lysis
   Acute osteomyelitis (see Fig. 4-22)

Calcifications

Calcifications are typically classified into three categories. The first is metastatic, a disturbance of Ca and PO_4 metabolism (Ca x PO_4 >60-70); the second is calcinosis, in which Ca and PO_4 metabolism is normal; and third, dystrophic, wherein calcium is deposited in devitalized tissues.

1. Associated pathologies with metastatic calcification
   Widespread bone resorption

Fig. 4-22. Focal osteopenia of the medial first metatarsal head in acute osteomyelitis. An erosion of the terminal phalangeal tuft is also apparent.

- Primary and secondary hyperparathyroidism
- Hypoparathyroidism
- Pseudohypoparathyroidism
- Massive bone destructive processes
- Metastatic tumors
- Multiple myeloma
- Leukemia
- Miscellaneous, such as gut absorption
- Sarcoidosis
- Hypervitaminosis D
- Idiopathic hypercalcemia
- Immobilization/paralysis
- Milk-alkali syndrome
- Cystic fibrosis
- Hyperphosphatemia

2. Idiopathic calcinosis
   - Calcinosis interstialis universalis
   - Tumoral calcinosis
   - Calcine peritendinitis and bursitis
3. Dystrophic calcification associations
   - Postinfection, infestation
   - Ehlers-Danlos syndrome
   - Neoplasms/tumor necrosis
   - Trauma
   - Connective tissue diseases
   - Vascular disease
   - Neuropathy
   - Hematoma
   - Injection sites
   - Blunt trauma
4. Generalized calcinosis
   - Calcinosis interstitialis universalis
     - Longitudinal direction, plaque-like
     - Skin and subcutaneous; occasionally tendons and muscles suggesting myositis, but no true bone formation occurs
   - Tumoral calcinosis
     - Often periarticular
     - Large, solid, lobulated
   - Collagen vascular diseases
     - Dermatomyositis
       - Fine, often reticular
       - Associated with malignancies
       - Often circumscribed (calcinosis circumscripta)
     - Scleroderma with calcinosis (Thibierge-Weissenbach syndrome)
       - Achilles tendon
       - Forefoot
       - Tuftal
       - Leg; streaky or diffuse linear
       - Circumscribed, lobulated or flocculent
5. Periarticular calcification(s)
   - Synovial osteochondromatoses
   - Calcific tendinitis
   - Collagen vascular diseases
   - Systemic lupus erythematosis
   - Hyperparathyroidism and renal osteodystrophy
   - Hypoparathyroidism
   - Hypervitaminosis D
   - Milk-alkali syndrome
   - Tumoral calcinosis
   - Calcinosis universalis
   - Articular disorders
     - CPPD
     - Calcium hydroxyapatite deposition
     - Gout
     - Infection

6. Bursal, tendinous, or ligamentous calcifications
   - Calcific bursitis
   - Gout and pseudogout (Fig. 4-23)
   - Hypervitaminosis D
   - Calcium hydroxyappetite deposition disease
   - Ochronosis, Wilson's disease
   - Secondary hyperparathyroidism (occasionally primary)
7. Acral calcification
   - Raynaud's disease
   - Systemic lupus
   - Scleroderma/CREST syndrome
   - Dermatomyositis
   - Calcinosis circumscripta universalis

Vascular Calcifications

1. Monckeberg's medial sclerosis
2. Calcific arteriosclerosis
3. Intravascular phleboliths (rare in forefoot)
   - Calcifications in veins
   - Maffucci syndrome when pedal involvement is extensive (hemangiomas)
   - Hemangioma

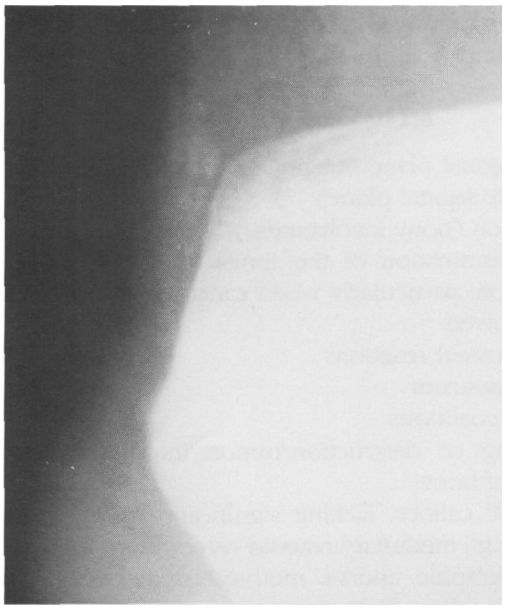

Fig. 4-23. CPPD. Note the fine, linear calcification in the achilles tendon.

4. Underlying calcifying disorder (especially secondary hyperparathyroidism in younger patients)
5. Premature atherosclerosis
   - Nephrotic syndrome
   - Hypothyroidism
   - Diabetes
   - Cushing syndrome

Soft Tissue Ossification

1. Neoplasm (e.g., parosteal osteosarcoma)
2. Post-traumatic ossification
3. Ossifying hematoma
4. Surgical scar
5. Severe burns
6. Paralysis
7. Myositis ossificans
   - Heterotopic ossification of soft tissue with metaplasia of the intermuscular connective tissue (not secondary to muscle inflammation)
8. Radiographic findings
   - Soft tissue mass, early (possible association with periostitis, 7-10 days)
   - Peripheral osteoid (lacy new bone) formation 4-6 weeks post injury
   - Lucent, cystic central changes
   - Maturity, 5-6 months; trabeculation apparent
   - Radiolucent band (zone) between myositic mass and subjacent bone cortex
   - Ectopic bone, usually lying along axis of involved muscle

Appearance of Loose Intra-Articular Ossific Bodies

1. Avulsion fracture
2. Synovial osteochondromatoses
3. Osteochondral fracture
4. Degenerative joint disease
5. Freiberg's infraction
6. CPPD
7. DISH

Dactylitis

1. Seronegative arthritis (with enthesopathy)
2. Sickle cell anemia
3. Spina ventosa/tuberculosis

4. Syphilis
5. Sarcoidosis (occasionally)
6. Traumatic periostitis

Coarsened Trabecular Pattern

1. Paget's disease
2. Hemoglobinopathies
3. Gaucher's disease

Heel Pad Thickening

This anomaly is defined with a non-weight-bearing lateral pedal view; in women, it is greater than 21 mm. and in men, greater than 23 mm.

1. Acromegaly
2. Dilantin therapy
3. Obesity
4. Peripheral edema
5. Myxedema
6. Infection

OVERVIEW OF PEDAL APPLICATIONS FOR THE NEWER, "STATE-OF-THE-ART" ANCILLARY IMAGING MODALITIES

Tomography: Overview and Advantages

Tomography is primarily indicated for imaging planar detail in areas of complex osseous anatomy. The tomographic principle allows for the "focusing-in" of a cross-sectioned anatomic plane by blurring all superimposed image detail outside of a predetermined focal plane. This focal plane lies at the system fulcrum, around which the x-ray tube head and film move in opposite directions. Those factors that increase the width of the blur (increasing angular arc, distance from film or focal plane), as well as the efficiency of blurring motion, improve the quality of the resultant studies.

Effective pedal imaging can usually be attained with either linear or circular tomography. However, the resolving power of complex or pleuridirectional (trispiral and hypocycloidal) tomography is superior to that of plain film radiography in that it is able to "efface" the overlying bony cortex to allow for visualization of internal medullary osseous lesions. With respect to image quality, the orientation of x-ray tube travel can be significant in that maximum blurring occurs when the longitudinal axis of the part to be studied is perpendicular to the direction of tube travel.

Most pedal techniques employ 0.5-cm-slice thickness with wide-angle tomography (30°- 50°). Wide-angle tomography is best for tissues with high inherent contrast (bone) but result in unacceptable soft tissue detail. In the foot, the true extent of geographic destruction within cancellous bone(s) may not be appreciated with plain film radiography. Tomography can often elucidate the extent of this involvement. However, prolonged exposure times to ionizing radiation are typically required. Largely replaced by computed tomography (CT) scanning, tomography of the foot still has one great advantage over modern CT scans, that is, the ability to directly image sagittal plane detail in all patients.

Primary Disadvantages of Tomography

1. Radiation dosage
2. Ghost images
3. Availability (particularly pleuridirectional units)
4. Poor soft tissue visualization
5. Superimposed blurring

Major Pedal Indications

1. Orthogonal plane imaging of the tarsal bones (especially sagittal plane)
2. Infection (bony involvement)
   - Determination of the limits/extent of destruction, particularly when cancellous bone is involved
   - Periosteal reactions
   - Sequestrum
3. Tarsal coalitions
4. Imaging of destruction/tumors/internal margination of bone
   - Small caliber, lacking significant osteosclerosis (e.g., medullary osteoid osteoma)
   - Geographic and/or moth-eaten destruction in cancellous bony areas
   - Cortical erosion
   - Matrix details inferior to CT scans

5. Postoperative complications
   - Bone graft incorporation
   - Metallic implant problems
6. Trauma
   - General evaluation of tarsal bony fracture(s)
   - Talar stiedas process fractures
   - Ankle joint pathology, e.g., osteochondral fractures
   - Evaluation of fracture healing or nonunions
7. Joints
   - Locate/identify juxta-articular and periarticular calcific and ossific bodies.
   - Evaluate joint space integrity of tarsal joints (complex anatomy).

Magnetic Resonance Imaging: Brief Overview

Magnetic resonance is the phenomenon of resonating interaction between magnets (magnetic materials or atoms) and magnetic fields. In essence, certain substances can undergo the absorption of energy from externally applied electromagnetic field waves when the frequency is properly "tuned." When properly tuned, just like sound waves resonating within a wine glass, all the atomic nuclei of a given species act in concert (spin coherently in "phase"). They simultaneously start to "tip" (perturb) in a different direction with an angle determined by the duration of application. The law of entropy dictates that these excited substances must release electromagnetic radiation of a similar frequency in returning to their original energy states when the radiofrequency field waves are no longer applied.

In applying this concept to the imaging of living tissues, the nuclei of certain atoms can behave like small magnets and develop "poles." These nuclei typically have unpaired protons or neutrons and therefore possess spinning electrical charges that generate a magnetic field. In selecting atoms to optimally image living tissues, one might intuitively look for atoms that emit the best (strongest) signals and are found throughout all body tissues; hydrogen, a component of water, proves to be the best choice.

When the patient is placed within the strong magnetic field gantry of the magnetic resonance image (MRI) scanner, hydrogen atoms tend to align and oscillate with the external magnetic field. Their oscillating frequencies (about 42.5 million cycles per second in a 1.0-tesla (T) magnet and 64 megahertz in 1.5 T), known as the Larmor frequency, fall into the radio wavelength bands of the electromagnetic spectrum. These nuclei are then stimulated (perturbed, tipped) by a series of short radio wave burst/pulse cycles to various tip angles; the hydrogen atoms then "relax" to their previous, unexcited alignments, concurrently emitting magnetic radiance signals. These data are then used to reconstruct an image.

The microenvironment of hydrogen may change from tissue to tissue throughout the body. This affects the behavior of the hydrogen atom during imaging and therefore the emitted signals after excitation. These effects can be observed through the measurement of Tl and T2 relaxation time constants of hydrogen for certain tissues. Simply put, one Tl interval represents an exponential regrowth constant in the original magnetic field direction and is the time it takes for hydrogen nuclei to emit 63 percent of the energy absorbed from the stimulating pulse. Tl time constant values are dependent on the external magnetic field strengths. One T2 interval represents the exponential decay of phase coherence in a plane perpendicular to the main magnetic field and is the time required for 63 percent of the signal to be lost by dephasing. T2 time constants are largely independent of the applied external magnetic field strength.

It is important to realize Tl and T2 relaxation times form the basis of tissue characterization and contrast. The values of Tl and T2 are approximately the same in pure water (e.g., urine and cerebrospinal fluid). In the complex microenvironments of living body tissues, water may be impure; it is often in solution, it can be in motion or tightly bound in a crystal lattice, or it may be attached to macromolecules, compartmentalized, subjected to thermal effects, viscosity, and so on. In contradistinction to pure water values, both Tl and T2 are greatly shortened and the signal fades correspondingly faster. The effects of flow are variable. Paramagnetic substances such as methemoglobin formation (old hematoma) or intravenous gadolinium injection shorten Tl and greatly shorten T2 relaxation times of tissues.

It is, however, impossible to discriminate between Tl and T2 effects with a single stimulating pulse because only regional hydrogen concentration would be measured. Discrimination is accomplished largely

through the employment of various radiofrequency pulsing techniques or the injection of paramagnetic contrast agents. With respect to pulse sequences, to evince these differences and therefore maximally contrast tissue signals, two or more pulses are applied in rapid succession. Employing such pulse sequences, images can be "weighted" to maximize either their Tl or T2 signal characteristics. The time interval between repetitive pulses is the "time to repeat" (TR) and the user-determined time interval between pulse and signal measurement or echo return from the patient is the "time to echo" (TE). In standard spin-echo pulse sequences, a short TR and TE will yield Tl-weighted images whereas a long TR and TE interval will yield T2-weighted images. Long TR and short TE times produce the "balanced," proton density image.

In general, a TR greater than 1.5 seconds (1,500 msec) and a TE greater than 0.4 seconds (40 msec) are considered long. Tl-weighted images are often acquired with 500/20 (millisecond) TR/TE combinations, respectively, and T2-weighted images with 2,000/80 TR/TE combinations, respectively.

Pathology often alters the normal relaxation time of a given tissue, and thus allows for this delineation from normal tissues. In general, shortened Tl and lengthened T2 relaxation times produce brighter signal intensities and vice versa. Although absolute signal intensities can change considerably with changes in both TR and TE, the relative intensities do not change significantly between many tissues.

It is standard procedure to employ spin-echo pulse cycle imaging in the foot to provide proton density (balanced), Tl- and T2-weighted images. Newer pulse-sequence methods are yielding exciting results while reducing MRI patient scanning times:

a. Short-tau inversion recovery techniques (STIR) are now performed along with Tl-weighted and T2 fat saturation images to improve the contrast between normal and pathologic tissues. Occasionally, in the workup of infection, STIR images along with only Tl images are acquired. In these instances, the addition of T2-weighted images may contribute useful information and eliminate some false-positive readings (e.g., septic arthritis with possible osteomyelitis).
b. Gradient-echo techniques (FLASH, GRASS) employ a single partial flip angle (usually from 5° to 30°) RF pulse along with two opposing magnetic gradients that first dephase and then ultimately rephase nuclei ("gradient reversal"). This yields a free induction decay (FID) echo. Depending on the technique, gradient-echo methods can substantially reduce MRI scan times (1 sec per scan is not uncommon). The signal intensities of tissues may vary in that marrow signals are typically darker and hyaline cartilage can be substantially brighter (from afar, these images may mimic T2-weighted spin-echo images). Soft tissue contrast is poor when compared to standard spin-echo imaging, although gradient-echo techniques can often improve imaging of hematoma and calcifications.
c. Saturation pulse sequence (e.g., CHESS) techniques can effectively cancel the signals emanating from protons bound to either fat or water in a given voxel. Additionally, post-contrast Tl with gadolinium-DTPA fat saturation often improves the Tl tissue (marrow) contrast.

Surface coils are commonly used to yield a small field of view (FOV) and maximize detail (maximize signal-to-noise ratio). The smallest coil possible should be employed to fit the body part in foot and ankle imaging. Two knee coils, and occasionally head coils, are used. Flat surface coils are often best for achilles tendon imaging. Even though MR imaging of the foot and ankle is now commonplace in podiatric medical practice, the practitioner must be wary of sending patients for scanning to hospitals or imaging centers that do not routinely perform pedal MR scans or to institutions that prefer not to do them. Studies are often suboptimal under these circumstances.

The MRI Gray Scale: Normal Signal Intensities

1. High intensity:
   Fat
   Marrow
2. Low to intermediate intensity:
   Muscle
   Hyaline cartilage
3. Very low intensity:
   Cortical bone
   Air
   Ligaments and tendons
   Fibrocartilage

4. Variable intensity (low-intensity Tl; high with T2):
   - Inflammatory or edematous tissue
   - Neoplastic tissue
   - Hemorrhage (interstitial)
   - Hematoma (intensity varies with age of hematoma)
     - Increased initial Tl and T2
     - Progressive decrease of Tl greater than T2 (effect seen with field strengths >1.0 T)
   - Fluid-filled structures

General Advantages of MRI

1. Superior soft tissue contrast
2. Safety (nonionizing)
3. Sensitivity to blood flow
4. Multiplanar/triplanar pedal imaging; true orthogonal planes can be acquired, any plane can be imaged
5. Contrast enhancement with minimal risk; contrast agents can be employed
6. Highly sensitive to many pathologies; however, not specific

Limitations of MRI

1. MRI has longer scanning times than CT. Newer pulse sequencing may soon minimize this problem.
2. Although the sensitivity for pathology often approaches 100 percent (e.g., osteomyelitis), the specificity is considerably less for many osseous abnormalities, particularly those involving abnormal marrow signals. In these instances, the morphologic appearance may be more reliable than the marrow signal.
3. Large metallic objects in the vicinity of the scanner, particularly ferromagnetic objects, can cause significant image disruption/distortion. In addition, a significant health hazard to the patient may occur with smaller ferromagnetic objects (orthopedic hardware, pellets) secondary to either dislodgment or heating during the actual scanning procedure.
4. Imaging of calcifications (except gradient echo/FLASH) is provided.
5. Negative imaging of the bony cortex is available.
6. Tissue heating occurs with MRI, although it is mild.
7. MRI is contraindicated with cardiac pacemakers.
8. MRI has a high cost.
9. MRI must be interpreted in the clinical context.

Common MRI Overlap (Look-Alike) Pathologies

1. Healed osteomyelitis
2. Fracture
3. Infarct
4. Diabetic neuropathic bone disease (noninfective bone disease; osteolysis)
5. Septic arthritis (may evoke abnormal signal intensities in adjacent bone marrow)

General Pedal Applications of MRI

1. Infection (osteomyelitis, cellulitis, absecesses)
2. Avascular necrosis
3. Reflex sympathetic dystrophy syndrome
4. Neoplasms (bony and soft tissue, including metastases and true neuroma from Morton's neuroma)
5. Hematoma
   - Fluid collections
   - Postoperative dead space
6. Joint Evaluation
   - Arthritis (low-signal synovial hypertrophy, cartilaginous narrowing)
   - Subchondral cysts
   - Internal derangements
   - Ligament (ankle) and tendon pathology
   - Tenosyovitis
   - Chronic tendinitis
   - Tendon rupture, total and partial
   - Effusion, bursitis
   - Fibrosis
7. Post-trauma
   - Stress fracture/insufficiency fracture
   - Osteochondritis dessicans (acute and old)
8. Marrow pathology
9. Nonmetallic foreign bodies; nonferromagnetic metallic foreign bodies

Computed Tomographic Imaging

The basic principle employed in computed tomographic (CT) scanning is that the internal structure of the body may be reconstructed in orthogonal planes by gathering attenuation data from multiple x-ray projections in many different directions. These x-ray beam scanning projections course through a fairly thin body plane, and the transmitted radiation registers with highly sensitive scintillation crystal detectors or

xenon gas ionization chamber detection systems. Since the inception of CT, each newer generation of CT scanners has resulted in dramatic decreases in overall scanning time over the previous generation. Concurrently, image quality has improved with advances in computers as well as their image reconstruction algorithms. "Pencil-thin" x-ray beams have been replaced with fan-shaped beams, and rotating detector systems have largely been supplanted by stationary rings of detectors lining the scanning gantry.

In CT image reconstruction, a body plane is subdivided into many smaller blocks of tissue (voxel; volume element) and then each block face (pixel on a picture screen readout) is assigned a number (linear attenuation coefficient) correlated to its x-ray beam attenuating power in that projection. These numbers, so-called "CT numbers," are based on the Hounsfield scale and allow the computer to assign gray-scale values to the image. Basically, the image may be centered around a given tissue's Hounsfield unit (either osseous or soft tissue) with a range of gray tones extending a variable, user-determined width (window width) above and below this numeric center point (window level). At the extremes of this range of gray tones are pure black and pure white. In common practice, bone and/or soft tissue windows are acquired.

Although MRI has largely replaced CT scanning for soft tissue and marrow imaging, CT scanning is superior in visualization of calcific and bony cortical lesions. Additionally, soft tissue-osseous interface pathology (e.g., tendinous impingement) may be accurately imaged with CT. Other pedal applications include diagnosing pathology not clearly delineated with plain film radiographs (usually occult around tarsal bones and ankle joint) and also surgical planning (e.g., osteochondritis dessicans, tumor, complex fractures, rearfoot surgery).

Overall Advantages of CT Scanning

Despite the following list of advantages, plain film radiographs should always be obtained before ordering CT scans.

1. Short scan times range between 1 and 5 seconds per slice.
2. Precise imaging of regional density differences. Newer CT scanners can measure tissue density to 1.0 Hounsfield units (1.0 H.U. = 0.1 percent of the density of water).
3. In comparison to conventional tomography, CT scanning offers the great advantage of producing cross-sectional images of superior contrast and detail without the superimposed blur or ghost image distortion.
4. In comparison with both conventional radiography and tomography, CT scans yield superior soft tissue contrast/delineation (through windowing) combined with the added capability of assigning Houndsfield (CT) attenuation values to pathologic tissue (Table 4-1). This can often help characterize the basic tissue makeup.
5. Three-dimensional CT imaging holds promise in the construction of preoperative models in areas of complex anatomy.
6. Although ancillary MRI has largely supplanted CT scanning of the soft tissue anatomy/pathology, in most aspects CT imaging remains a superior imaging modality for imaging of the skeletal system and soft tissue calcifications/ossifications.
7. CT can be used with cardiac pacemakers.
8. CT can be used with ferromagnetic materials.
9. CT may also be used with contrast studies such as arthrography.

Overall Limitations of CT Scanning

1. X-ray image has limitations; image is generally inferior to MR imaging soft tissue contrast.
2. CT scans produce ionizing radiation with potential long-term effects.
3. Pregnant female patients should not be scanned unless absolutely necessary.
4. Invasive contrast studies are often routinely employed.

Table 4-1. Hounsfield Units
(quantized attenuation values)

Heavy metal	>>> 1,000
Compact/cortical bone	1,000
Calcification	200 – 800 (600–1,000)
Clotted blood	40 – 60
Blood	25 – 40
Muscle	20 – 40
Water	0
Fat	-20 – -100
Air	-1,000

5. Physical constraints of the scanning gantry limits imaging to predominantly the transverse plane.
6. *Sagittal plane imaging of the foot cannot generally be obtained directly.* Basic CT scanner design precludes direct sagittal plane imaging of the foot in most patients. Although the computer is capable of reformatting (reconstructing) those anatomic planes not directly imaged, such images suffer from significant degradation of image quality. However, in about 30 to 40 percent of patients, direct sagittal plane imaging can be accomplished via internal (occasionally external) leg rotation with the knees flexed.
7. CT scanning is not devoid of some significant reconstruction artifacts; some of the more important ones include motion artifacts, streak artifacts, and beam-hardening artifacts. Note: Although the presence of a ferrometallic object(s) does not preclude scanning, streak artifacts of many metallic objects may significantly distort or totally obscure image detail (even more than MRI) when the object is large and lies within the image plane.

Common Pedal Applications for CT Scanning

1. Bony cortex/cortical pathology
2. Calcifications
3. Evaluation of neoplasms (H.U. assignments) (particularly bone tumors)
   - Internal margination/destructive typing
   - Matrix
   - Periosteal reaction
4. Trauma/nonunion
   - Tarsal bony fractures
   - Fractures of the os calcis (tendinous impingement)
   - Osteochondritis dessicans
   - Lisfranc fracture evaluation (image fracture pattern/elucidate osseous fragments)
5. Infection (especially chronic)
   - Involucrum
   - Cortex/sequestrum
   - Abscesses/plantar space infections
6. Joints
   - Subtalar joint arthritis
   - Evaluation of tarsal coalitions
   - Prosthesis (may be limited by artifacts)
   - Charcot joints (to ascertain degree of lysis, elucidate loose bodies, etc.)
7. Infarction
   - Osteonecrosis of navicular
   - Distal tibia
8. Muscles (pyomyositis)

BRIEF REVIEW OF RADIOGRAPHIC BIOMECHANICAL EVALUATION

The biomechanical evaluation is performed from the anteroposterior and lateral pedal radiographs. Standardization of foot position is essential for biomechanical radiographic evaluation. The accepted standard in podiatric medicine is proper placement of the patient in their midstance angle and base of gait. Inasmuch as first and fifth ray angles, indices, and bunion criteria are reviewed elsewhere in this text, they are not covered in this section. The succeeding axis descriptions should not be construed as axes of motion.

Anteroposterior View

1. Metatarsus adductus angle (Fig. 4-24)
   - Usual upper limit: 14°-17°
   - Normal adult range: 5°-17°
   - Pathologic: >20°
   - Values increase slightly with supination and decrease moderately with pronation.
   - Method (Fig. 4-24)
     - The angle is formed by the longitudinal axis of the lesser tarsus and the second metatarsal longitudinal axis. A transection to the lesser tarsal bones must first be constructed by identifying the four corners of a trapezoid that approximates these bones. Care must be taken not to utilize the lateral fourth metatarsocuboid joint margin or the styloid process of the fifth metatarsal base.
   - Alternate method (Engel et al; not depicted)
     - The four corners of the second cuneiform are defined by points, and a longitudinal bisection to this cuneiform is then constructed. The intersection of this bisection with the bisection of the second metatarsal bone defines the metatarsus adductus angle. This

Fig. 4-24. The metatarsus adductus angle.

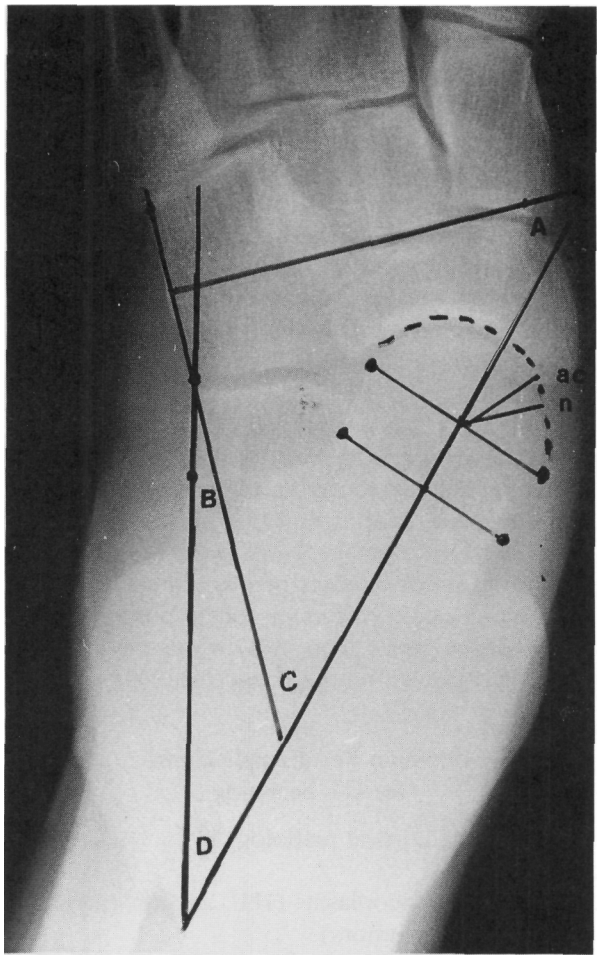

Fig. 4-25. Line AC is drawn to actual point of talonavicular articulation; line N is drawn to the average normal point spanning 75 percent of the articular surface of the taler head. Angle A is the talonavicular angle; B, the cuboid abduction angle; C, the talocuboid angle; D, the talocalcaneal angle.

method is much faster and reliably produces angular values about 3° higher than method (a).

2. Talocalcaneal angle (Fig. 4-25) (angle of Kite; Harris-Beath angle)

Normal ranges

Infants, 30°-50°
Age 1-10, about 30°
Adolescents >5 years, 20°-35°
Adults, 17°-21°

Decreased in subtalar joint supination

The angle is formed by the intersection of the longitudinal bisection of the talar neck (column tali) and longitudinal axis of the rearfoot. The longitudinal calcaneal axis (column calcanei) is typically substituted for the longitudinal rearfoot axis. This axis can be constructed with either a line parallel to the anteriolateral surface of the

calcaneus or perpendicular to the plane of the inferior calcaneocuboid articulation

3. Cuboid abduction angle (calcaneocuboid angle) (see Fig. 4-25)
   Normal range: 0°-5°
   Increased with midtarsal joint pronation
   Decreased with midtarsal joint supination
   The angle is formed by the intersection of the column calcanei and the longitudinal axis of the cuboid. A line drawn parallel to the lateral surfaces of each of these bones usually suffices (in lieu of geometric bisection).
4. Talonavicular angle (see Fig. 4-25)
   Normal range: 70° ± 10°
   Increased in supination
   Decreased in pronation
   The angle is formed by the column tali and the transection of the lesser tarsal bones.
   Alternate method
   The angle is formed by the bisection of the talar neck and a tangent to the proximal effective articular surface of the navicular. Inasmuch as the concave portion of any convex-concave articulation typically displays a thin subchondral sclerotic line spanning the joint, this easily delineates the effective articular surface. Although this method is faster, it is less commonly employed.
5. Talonavicular articulation (percent articulation of talus)
   Normal range: 75 percent of talar head articulates with navicular
   Decreases in pronation
   Increases in supination
   Inasmuch as the articulating surface limits of the talar head must be defined to form the distal bisecting segment of the column tali, the percent of talonavicular articulation can be accurately approximately by creating 45° angles to the midpoint of this segment (see Fig. 4-25).
6. Talocuboid angle (see Fig. 4-25)
   Normal range: 31° ± 2°
   Increases in pronation
   Decreases in supination
   Possible associations (36° moderate increase in IM)
   The angle is formed by the intersection of the longitudinal bisection of the talus and a line drawn parallel to the lateral surface of the cuboid.
7. Forefoot adductus angle (Fig. 4-26)
   Normal range: 0°-10°
   The angle is formed by the intersection of the column calcanei (or longitudinal axis of rearfoot,

Fig. 4-26. The forefoot adductus angle. A comparison of two different methods of forming the longitudinal rearfoot axis yields two parallel lines in this case.

when obtainable) and the longitudinal axis of the second metatarsal.

Lateral View

1. Lateral cyma line (Fig. 4-27)
   Normal range: Two continuous/conjoined hyperbolic curves
   Anterior break: Pronation
   Posterior break: Supination
   An ideally continuous S -shaped line formed by a tracing through the talonavicular and calcaneocuboid articular surfaces. Disruption is suggestive of abnormal rearfoot/subtalar joint mechanics. When a discontinuity occurs, the relative position of the talonavicular joint surface with respect to the calcaneocuboid joint surface determines the naming of the "break" (anterior or posterior). Invariably, when the arc formed by the talonavicular surface transects the calcaneocuboid joint, the cyma line is anterioinferiorly displaced. With a posterior cyma line, the two joint surface tracings do not intersect.
2. Talar declination angle (Fig. 4-28)
   Normal range: 21° ± 4°
   Increases in pronation
   Decreases in supination
   The angle is formed by the intersection of the lateral talar axis (column tali) and the weight-bearing reference line. The talar declination angle equals the lateral talocalcaneal angle minus the calcaneal inclination angle.
3. Calcaneal inclination angle (see Fig. 4-28)
   Normal range: 18°-23°
   0°-10°, very low (flatfoot)
   10°-20°, low to medium
   20°-30° medium
   >30°, high (posterior pes cavus)
   The angle is formed by the intersection of the weight-bearing reference line and a line connecting the most posterior inferior point of the os calcis with the anterior inferior osseous limit of the os calcis at the calcaneocuboid joint. Older methods suggest this line connect the posterior inferior and the anterior inferior osseous landmarks of the calcaneus.
4. Lateral talocalcaneal angle (see Fig. 4-28)
   Normal range: 45° ± 3°
   Increases in pronation
   Decreases in supination
   The angle is formed by the intersection of the column tali and the column calcanei. This be-

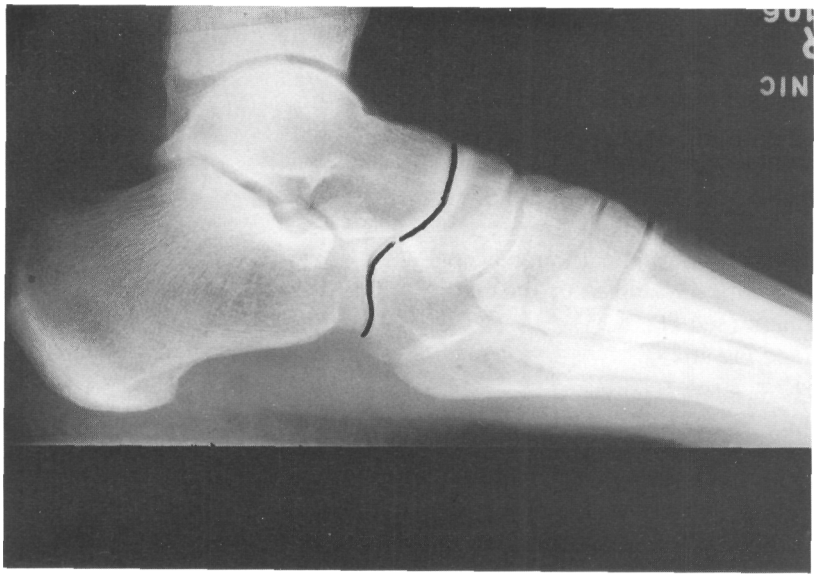

Fig. 4-27. A normal cyma line.

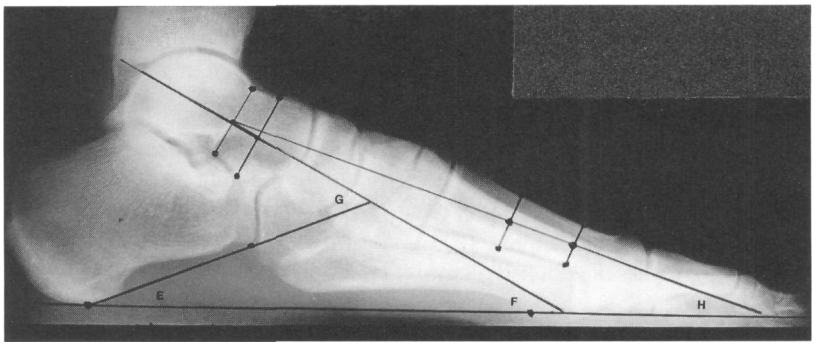

Fig. 4-28. Angle E is the calcaneal inclination angle; F, the talar declination angle; G, the lateral talocalcaneal angle; H, the metatarsal (first) declination angle.

comes the external angle of a triangle with opposite angles of talar declination and calcaneal inclination angle. The lateral talocalcaneal angle therefore equals talar declination plus calcaneal inclination angles.

5. Metatarsal declination angle(s) (see Fig. 4-28)
   Normal ranges (from S. Fuson and S. Smith)
   23° ± 8°, first metatarsal
   25° ± 4°, second metatarsal
   15° ± 4°, fifth metatarsal
   Increases in supination/pes cavus
   Decreases in pronation/flatfoot
   The angle is formed by the intersection of the longitudinal axis of the respective metatarsal and the weight-bearing reference line.
6. Lateral talometatarsal angle (not depicted) (talo-first metatarsal angle; Meary's angle)
   Normal range: 0°-14°
   15° or greater: cavus foot
   Age 5 years or less: negative angle
   Adult negative angle: pronation/flatfoot
   The angle is formed by the intersection of the lateral talar axis and the longitudinal bisection of the first metatarsal. The intersection of these two lines suggests the apex of deformity, particularly in cavus foot deformities. In a rectus foot, the column tali typically passes through the first metatarsal. In a pronated foot (or metatarsus primus elevatus), the column tali passes inferior to the first metatarsal head and vice versa with anterior cavus/supination.
7. Posterior Facet (declination) angle (not depicted)
   Normal range Approximately 45°
   Increases in pronation
   Decreases in supination
   The posterior facet angle, which is formed by the intersection of a line tracing through the posterior facet and the weight-bearing surface, is a gross indicator of pathology.

SUGGESTED READINGS

General

Aegerter E, Kirkpatrick JAJr: Orthopedic Diseases. WB Saunders, Philadelphia, 1975

Berquist TH: Radiology of the Foot and Ankle. Raven Press, New York, 1989

Brower A: Arthritis in Black and White. WB Saunders, Philadelphia, 1988

Chapman S, Nakielny R: Aids to Radiological Differential Diagnosis. Bailliere Tindall, London, 1990

Dahnert W: Radiology Review Manual. Williams & Wilkens, Baltimore, 1991

Edeiken J: Roentgen Diagnosis of Diseases of Bone. Williams & Wilkins, Baltimore, 1989

Felson B, Reeder M: Gamuts in Radiology. Audiovisual Radiology of Cincinnati, Cincinnati 1987

Forrester DM, Kricun ME: Imaging of the Foot and Ankle. Aspen. 1988

Greenfield G: Radiology of Bone Disease. JB Lippincott, New York, 1990

Keats T: An Atlas of Normal Roentgen Variants That May Simulate Disease. Year Book Medical Publishers, Chicago, 1984

Kinsman S, Kroeker R: Leg-Podiatry Radiography. California State Dept. of Health, Sacramento, California, 1973

McCarty DJ: Arthritis & Allied Conditions. Lea & Febiger, Philadelphia, 1985

Meschan I: Roentgen Signs in Diagnostic Imaging. Vol. 2. Appendicular Skeleton. WB Saunders, Philadelphia, 1985

Montagne J, Chevrot A, Galmiche JM: Atlas of Foot Radiology. Masson, New York, 1981

Ravin CE, Cooper C: Review of Radiology. WB Saunders, Philadelphia, 1990

Resnick D: Common disorders of synovium-lined joints: pathogenesis, imaging abnormalities, and complications. AJR 151:1079, 1988

Resnick D, Niwayama G: Diagnosis of Bone and Joint Disorders. Vols. 1-6. WB Saunders, Philadelphia 1988

Sartoris DJ, Resnick D: Radiological evaluation of patients with arthritis. Pathol Annu 86:293, 1986

Silverman FN: Caffey's Pediatric x-ray diagnosis. Yearbook Medical, Chicago, 1985

Weissman S: Radiology of the Foot. Williams & Wilkins, Baltimore, 1989

Ancillary Imaging Modalities

Berquist TH: Magnetic Resonance of the Musculoskeletal System. Raven Press, New York, 1987

Curry TS, Dowdey JE, Murry RC Jr: Christensen's Physics of Diagnostic Radiology, Lea & Febiger Philadelphia, 1990

Edelman R, HesselinkJR: Clinical Magnetic Resonance Imaging. WB Saunders, Philadelphia, 1990

Horowitz AL: MRI Physics for Radiologists. A visual Approach. Springer-Verlag, New York, 1992

Hounsfield GN: Computerized transverse axial scanning (tomography). Br J Radiol 46:1016, 1973

Oloff-Solomon J, Solomon MA: Computed tomographic scanning of the foot and ankle. Clin Podiat Med Surg 5:931, 1988

Oloff-Solomon J, Solomon MA: Magnetic Resonance Imaging in the Foot and Ankle. Clin Podiatr Med Surg 5:945, 1988

Resnick D: Bone and Joint Imaging. WB Saunders, Philadelphia, 1989

Wolf GL, Popp C: NMR—A Primer for Medical Imaging. Slack, Thorofare, NJ, 1984

Biomechanics

Altman ML: Sagittal plane angles of the talus and calcaneus in the developing foot. J Am Podiatry Assoc 58:191, 1968

Coleman SS: Complex Foot Deformities in Children Lea & Febiger, Philadephia, 1983

DiGiovanni JE, Smith SD: Normal biomechanics of the adult rearfoot. J Am Podiatry Assoc 66:812, 1976

Engel E, Erlick N, Krems I: A simplified metatarsus adductus angle. J Am Podiatry Assoc 73:620, 1983

Fuson SM, Smith SD: Angular relationships of the metatarsal, talus, and calcaneus. J Am Podiatry Assoc 68:463, 1978

Gamble FO, Yale I: Clinical Foot Roentgenology. Kreiger, Huntington, NY, 1975

Giannestras JJ: Foot Disorders: Medical and Surgical Management. Lea & Febiger, Philadelphia, 1973

Greenberg GS: Relationship of Hallux Abductus Angle and First Metatarsal Angle to Severity of Pronation. J Am Podiatry Assoc 69:29, 1979

Kaschak TJ, Laine W: Surgical radiology. Clin Podiatr Med Surg 5:797, 1988

LaPorta GA, Scarlet J: Radiographic changes in the pronated and supinated foot. J Am Podiatry Assoc 67:334, 1977

Meary R: On the measurement of the angle between the talus and the first metatarsal. Symposium sur le pied creux essentiel. Rev Chir Orthop 53:389, 1967

Montagne J, Chevrot A, Galmiche JM: Atlas of Foot Radiology. Masson, New York, 1981

Root ML, Orien WP, Weed JH: Clinical Biomechanics. Vol. II. Normal and Abnormal Function of the Foot. Clinical Biomechanics, Los Angeles, 1977

Sgarlato TE: A Compendium of Podiatric Biomechanics. California College of Podiatric Medicine, 1971

Solomon M: Roentgenographic Biomechanical Evaluation of the Foot. Johnathan Douglass, 1973

Templeton AW, McAlister WH, Zim ID: Standardization of terminology and evaluation of osseous relationships in congenitally abnormal feet. AJR 93:374, 1965

Whitney AK: Radiographic Charting Technique. Pennsylvania College of Podiatric Medicine, 1978